

Article

Flow Field Analysis and Feasibility Study of a Multistage Centrifugal Pump Designed for Low-Viscous Fluids

Mohamed Murshid Shamsuddeen ^{1,2} , Sang-Bum Ma ², Sung Kim ², Ji-Hoon Yoon ³, Kwang-Hee Lee ⁴, Changjun Jung ⁴ and Jin-Hyuk Kim ^{1,2,*} 

¹ Industrial Technology (Green Process and Energy System Engineering), Korea University of Science & Technology, Daejeon 34113, Korea; murshishams@kitech.re.kr

² Clean Energy R&D Department, Korea Institute of Industrial Technology, Cheonan-si 31056, Korea; sbma@kitech.re.kr (S.-B.M.); ks2928@kitech.re.kr (S.K.)

³ Dongyang Chemical Pump Company, Paju-si 10832, Korea; isimi@dycp.co.kr

⁴ GS Caltex Corporation, Seoul 06141, Korea; kayhlee@gscaltex.com (K.-H.L.); cjjung@gscaltex.com (C.J.)

* Correspondence: jinhyuk@kitech.re.kr; Tel.: +82-41-5898447

Featured Application: The proposed multistage centrifugal pump design can be applied to satisfy the high head and high flow rate requirements in chemical processing industries.

Abstract: A multistage centrifugal pump is designed for pumping low-viscosity, highly volatile and flammable chemicals, including hydrocarbons, for high head requirements. The five-stage centrifugal pump consists of a double-suction impeller at the first stage followed by a twin volute. The impellers for stages two through five are single-suction impellers followed by diffuser vanes and return channel vanes. The analytical performance is calculated initially in the design stage by applying similarity laws to an existing scaled-down pump model designed for low flow rate applications. The proposed pump design is investigated using computational fluid dynamics tools to study its performance in design and off-design conditions for water as the base fluid. The design feasibility of the centrifugal pump is tested for other fluids, such as water at a high temperature and pressure, diesel and debutanized diesel. The pump design is found to be suitable for a variety of fluids and operating ranges. The losses in the pump are analyzed in each stage at the best efficiency point. The losses in efficiency and head are observed to be higher in the second stage than in other stages. The detailed flow behavior at the second stage is studied to identify the root cause of the losses. Design modifications are recommended to diminish the losses and improve the overall performance of the pump.

Keywords: multistage centrifugal pump; double-suction impeller; twin volute; computational fluid dynamics; design feasibility study



Citation: Shamsuddeen, M.M.; Ma, S.-B.; Kim, S.; Yoon, J.-H.; Lee, K.-H.; Jung, C.; Kim, J.-H. Flow Field Analysis and Feasibility Study of a Multistage Centrifugal Pump Designed for Low-Viscous Fluids. *Appl. Sci.* **2021**, *11*, 1314. <https://doi.org/10.3390/app11031314>

Academic Editor: Kambiz Vafai

Received: 26 December 2020

Accepted: 26 January 2021

Published: 1 February 2021

Publisher's Note: MDPI stays neutral with regard to jurisdictional claims in published maps and institutional affiliations.



Copyright: © 2021 by the authors. Licensee MDPI, Basel, Switzerland. This article is an open access article distributed under the terms and conditions of the Creative Commons Attribution (CC BY) license (<https://creativecommons.org/licenses/by/4.0/>).

1. Introduction

One of the most commonly used turbomachines in chemical and petroleum industries is the multistage centrifugal pump. In the construction of potential infrastructure for chemical processing, multistage centrifugal pumps still play an important role. They are usually employed for high-head applications, such as in boilers and power plants. They are capable of handling low-viscous, volatile and flammable fluids and can operate in temperature ranges from $-120\text{ }^{\circ}\text{C}$ to $370\text{ }^{\circ}\text{C}$ [1]. Here, low-viscous fluids refer to fluids having viscosities lower than normal water. Compared to single-stage pumps, the efficiency, reliability and performance of these pumps are substantially more important because of the extreme operating conditions. Consequently, it is necessary to be aware of the turbulent fluid flow behavior inside the pump in the design stage itself. This can be achieved by careful consideration of all the stages in the planning, design and testing in both design and off-design conditions. Manufacturers turn to computational methods to test design

features, decrease the number of experimental tests conducted and identify undesirable design features at an early stage to save resources and time.

Computational fluid dynamics (CFD) tools are used by turbomachinery designers to design pumps that function more efficiently. Modern pumps are first designed theoretically, tested using CFD tools and then by laboratory experiments. The laboratory-tested pumps are again studied using CFD simulations, and optimization strategies are applied for improving the pump's performance before manufacturing. Samad et al. [2–4] used CFD simulations to design, test and optimize centrifugal pumps for pumping multiple fluids used in the oil and gas industries. Hamid et al. [5–7] tested centrifugal pumps used for pumping water and light crude oil through experimental analysis and optimizing them using CFD tools. Watanabe et al. [8,9] studied the forces in a three-stage centrifugal pump at design and off-design conditions using CFD simulations. Pumps are designed to withstand high temperatures and pressures, and they are able to pump fluids of different densities and viscosities.

Several multistage centrifugal pump designs are available on the market for the transportation of chemicals [10,11], although a new pump design is required for pumping perilous chemicals with high head and high flow rate requirements in petrochemical refineries. The proposed pump design consists of a double-suction impeller and a twin volute at the first stage. A single-suction impeller with a diffuser and return vanes are added to Stages 2–4. Stage 5 consists of an impeller followed by diffuser blades and an outlet volute.

A double-suction impeller design is chosen for the first stage due to the back-to-back arrangement of the two impellers. This arrangement provides a zero average axial force [12]. Double-suction impellers are used in centrifugal pumps for obtaining large flow rates, improving suction performance, reducing axial thrust on the bearings and cutting down capital cost [13]. The fluid enters independently into the two suctions and flows into the impellers. The fluid leaves the impellers together into the volute. Although the axial force of the double-suction impeller is theoretically balanced, it is not possible to overlook the radial forces. Two strategies can be used to decrease the impeller radial force of the double-suction stage. One is using a staggered impeller that has been studied previously [14,15] while the other is to use a twin-volute casing. Kang et al. [16] studied the effects of a twin volute in a submersible centrifugal pump and obtained a uniform distribution of high absolute velocity in the volute, homogeneously distributed flow structures and a flat high-velocity profile at the volute throat. Mina et al. [17] used a triple-volute casing design to reduce the radial thrusts in a single-stage centrifugal pump. Although a more uniform pressure distribution is offered by three volutes, the design is not feasible in multistage centrifugal pumps. Suzuki et al. [18] studied the performance of a five-stage, high-pressure volute pump having a twin volute with crossovers between stages. The long crossovers, in addition to the twin volute, caused fluid pre-rotation opposite to the impeller's rotational direction. Teesink et al. [19] optimized the twin-volute crossover design to improve efficiency by 3%. The optimization resulted in a decrease of the pre-swirl replacing the suction splitters. The design recommendations from these works encouraged the development of a twin-volute design staggered by 180° without the use of long crossovers. The high-speed fluid from the impeller enters the twin volute and passes the fluid onto the second stage. The twin volute design offsets the radial forces to each other [20].

The design feasibility study of a multistage pump designed for pumping hazardous fluids in petrochemical refineries with high head and high flow rate requirements is presented in this paper. The operability of the pump is tested for multiple fluids using CFD simulation techniques. The loss analysis of the proposed design is carried out for individual stages and, accordingly, design modifications are recommended.

2. Description of the Pump Model

Multistage pumps are used when a high discharge pressure is required, but it is beyond the duty range of single-stage pumps. There are several factors to consider while

choosing the number of stages required for the pump model. The number of stages is determined by the head requirement, the Net Positive Suction Head Required (NPSHr), the minimum flow requirement and the performance curve. The more stages a pump has, the higher the final discharge pressure. The proposed multistage pump is designed in such a manner that the number of stages can be increased or decreased, depending on the requirements. A five-stage pump is chosen here to meet the high head and flow rate requirements of several units in the petrochemical refinery.

The five-stage centrifugal pump model consists of a double-suction impeller and a twin volute staggered at 180° in the first stage. The suction chamber has a semispherical shape, with baffle plates installed near the inlet of the double-suction impeller to reduce any possible swirling action toward the impeller inlet. The second stage consists of an impeller, diffuser and return vane. Stages three and four are the repetition of the second stage. An impeller, diffuser and outlet volute are installed in the fifth stage. The impeller is designed to attain a high head with optimum efficiency, while the diffuser is intended to maximize the pressure in the diffuser vanes and minimize the pressure gradient in the return vanes. The pump design indicating each component is shown in Figure 1. The preliminary design of the pump model was obtained from a dynamically similar existing pump provided by the manufacturer. The existing pump was a scaled-down model used for non-hazardous fluids in low flow rate applications. The proposed pump is specifically scaled-up for handling hazardous fluids at a high flow rate and high head operation. The design is extracted using pump affinity laws as shown below:

$$\frac{Q_1}{Q_2} = \left(\frac{n_1}{n_2}\right); \frac{H_1}{H_2} = \left(\frac{n_1}{n_2}\right)^2; \frac{P_1}{P_2} = \left(\frac{n_1}{n_2}\right)^3 \quad (1)$$

where the quantities denoted by subscriptions 1 and 2 refer to the model and the prototype. The quantities n , Q , H and P correspond to the rotational velocity, flow rate, head and input power, respectively.

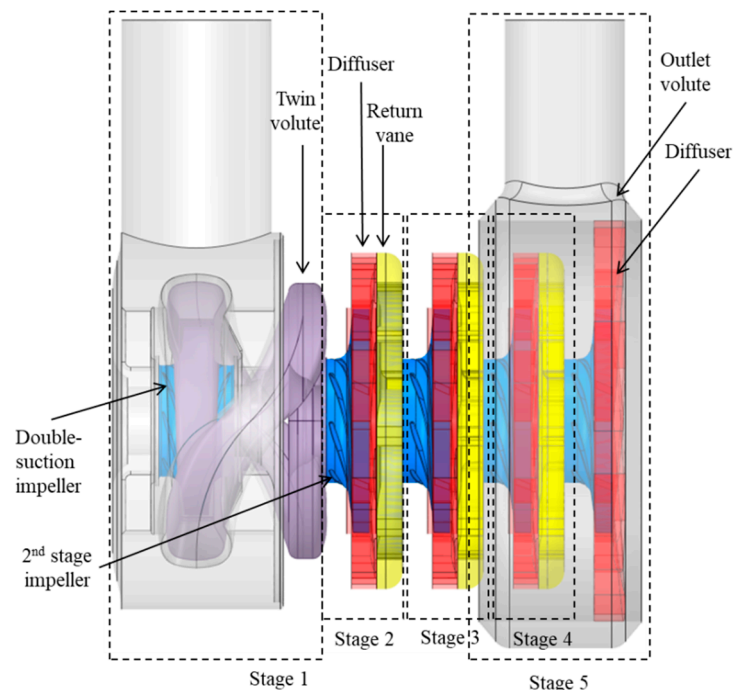


Figure 1. The multistage centrifugal pump design.

The impeller blade, diffuser vanes and return vanes were designed using BladeGen software. BladeGen is a comprehensive blade design tool commonly used by turbomachin-

ery designers for the design and control of a blade’s properties, including but not limited to the meridional shape, blade angles, thickness and cut-offs [21]. The meridional view of the blades is shown in Figure 2. The design specification of the multistage centrifugal pump is given in Table 1.

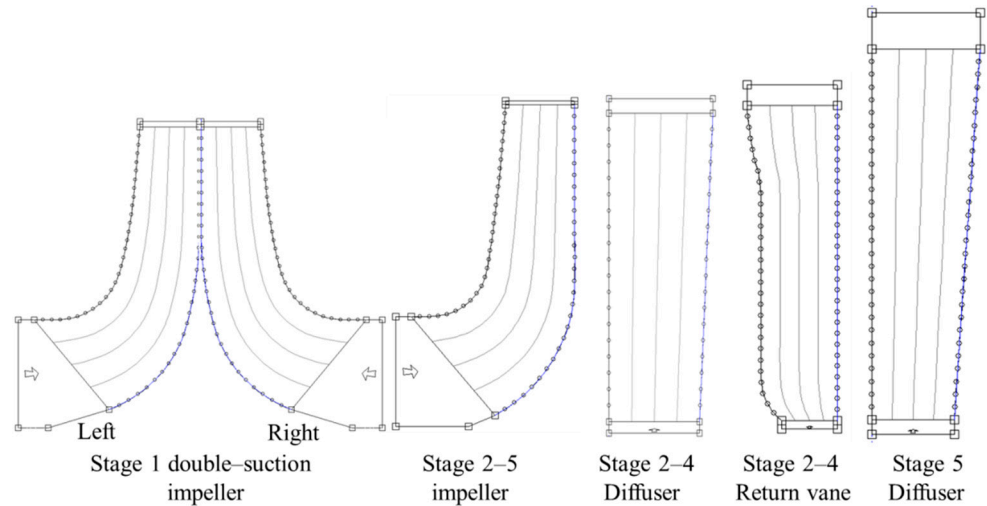


Figure 2. The meridional shape of the rotating blades and stationary vanes.

Table 1. Pump specification.

Parameter	Value	Parameter	Value
Number of stages	5	Initial working fluid	Water
Flow coefficient (φ)	0.01	Impeller diameter (Stage 1)	D
Head coefficient (ψ)	0.67	Impeller diameter (Stage 2–5)	1.2 D

The head coefficient and the flow coefficient are calculated using the following relations [22]:

$$\psi = \frac{gH}{n^2 D^2} \tag{2}$$

$$\varphi = \frac{Q}{nD^3} \tag{3}$$

where ψ is the head coefficient, φ is the flow coefficient, D is the impeller diameter and g is the acceleration due to gravity.

The pump performance is calculated theoretically using the parameters obtained from Equation (1), and the efficiency is calculated using Equation (4):

$$\eta = \frac{\rho Q g H}{P} \tag{4}$$

Figure 3 shows the pump performance curve obtained by theoretical calculations. The preliminary design was tested for water, as the affinity laws were guaranteed for water or pure liquids with kinematic viscosities less than 10 cS [23]. The efficiency, dimensionless groups and head and flow coefficients were normalized using the values associated with the design point of the pump, which corresponded to the best efficiency point (BEP) of the pump. The H_{max} and H_{min} correspond to the head of the maximum and minimum impeller diameters, respectively. The head obtained by the actual pump operation must be between these values.

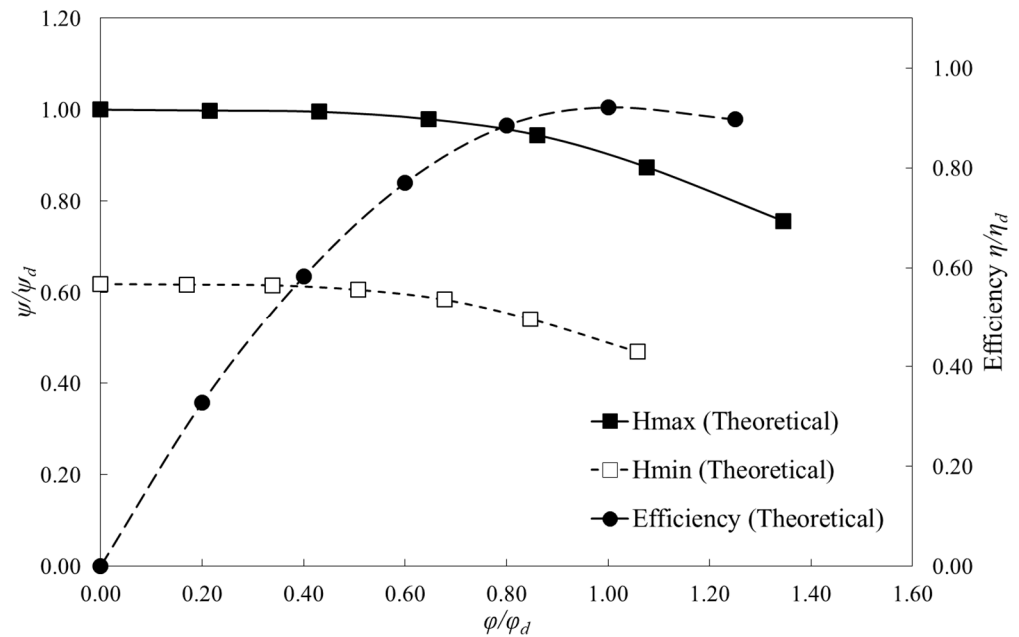


Figure 3. The theoretical performance curve of the pump design.

3. Numerical Model

The flow phenomena inside the pump were modeled by solving 3D mass and momentum equations in a commercial CFD code. The analysis was based on the steady, incompressible Reynolds-averaged Navier–Stokes (RANS) equations along with the $k-\omega$ based shear stress transport (SST) turbulence model, using a finite-volume solver provided in the commercial code ANSYS CFX 19.1. The SST model uses an integrated function to switch from the standard $k-\omega$ model near the wall region to a high Reynolds number form of the $k-\epsilon$ model away from the boundary layer [24]. The turbulence model was chosen based on similar studies by the authors for a three-stage centrifugal pump [25,26]. The mass conservation equation and the momentum conservation equation of the RANS can be written as

$$\frac{\partial \bar{v}_i}{\partial x_i} = 0 \tag{5}$$

$$\rho \frac{\partial \bar{v}_i}{\partial t} + \rho \frac{\partial (\bar{v}_i \bar{v}_j)}{\partial x_j} = -\frac{\partial \bar{P}}{\partial x_i} + \frac{\partial}{\partial x_j} [\mu (\frac{\partial \bar{v}_i}{\partial x_j} + \frac{\partial \bar{v}_j}{\partial x_i}) - \rho (\bar{v}_i \bar{v}_j)] \tag{6}$$

where, ρ , P , μ and v_{ij} represent the density, pressure, dynamic viscosity and velocity components, respectively. The overbar (–) denotes the average quantity.

The entire fluid domain in the computational model included the inlet domain, double-suction impeller, twin volute, single-suction second stage impeller, diffuser vanes, return channel vanes, Stage 3 and 4 domains, fifth stage impeller, diffuser and outlet domain. The impeller domains were rotating domains, while all other domains remained stationary. The impeller, diffuser and return channel domains were chosen as a single passage because of the periodically repeating nature of the domains. The periodic boundary condition saved the computational time required for a converged solution without compromising the accuracy of the results [27]. The outlet domain was extended to avoid any possible backflow phenomena at the pump outlet. The ambient pressure inlet and mass flow outlet were chosen for the boundary conditions. The interfaces between the rotating and stationary domains were taken as a stage (mixing-plane) model for the steady-state calculations due to the high pitch ratio between the domains. The interfaces between the stationary domains were chosen as a general connection with the general grid interface (GGI) mesh connection.

The numerical meshes for the fluid domains were generated using ANSYS meshing module for the stationary domains. The rotating impeller domain meshes are created using

Turbogrid software which provides high-quality hexagonal meshes with boundary layer control. To resolve the boundary layers, multiple layers of boundary meshes are installed along the blade suction and pressure side surfaces to keep the y^+ value below 30. Similar boundary layer meshes were also given for diffuser and return channel vanes.

The generated meshes were tested for grid independency to obtain the optimum mesh and reduce the influence of the grid density on the flow field. The tests were carried out for the design point using water as the initial fluid. The grid independence study was carried out for Stages 1 and 2 separately to find the optimum grid for the first and second stage impellers. Determining the optimum grid for the first and second stage was deemed adequate for the entire pump model, since the third, fourth and fifth stage geometries were a repetition of the second stage. The mesh of the outlet domain in the fifth stage was generated in a similar way to the inlet domain in the first stage. Figure 4 shows the grid independency test results for Stages 1 and 2 plotted against efficiency. The optimum meshes thus obtained were used to create the entire domain, and the total number of meshes generated for the full stage was 6.25 million nodes. The final mesh of the entire domain, the double-suction impeller and the twin-volute meshes are shown in Figure 5.

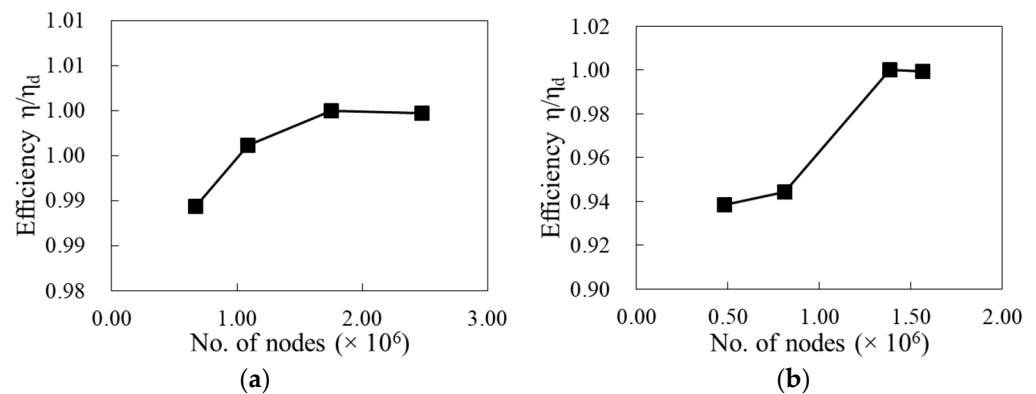


Figure 4. Grid independency test for (a) Stage 1 and (b) Stage 2.

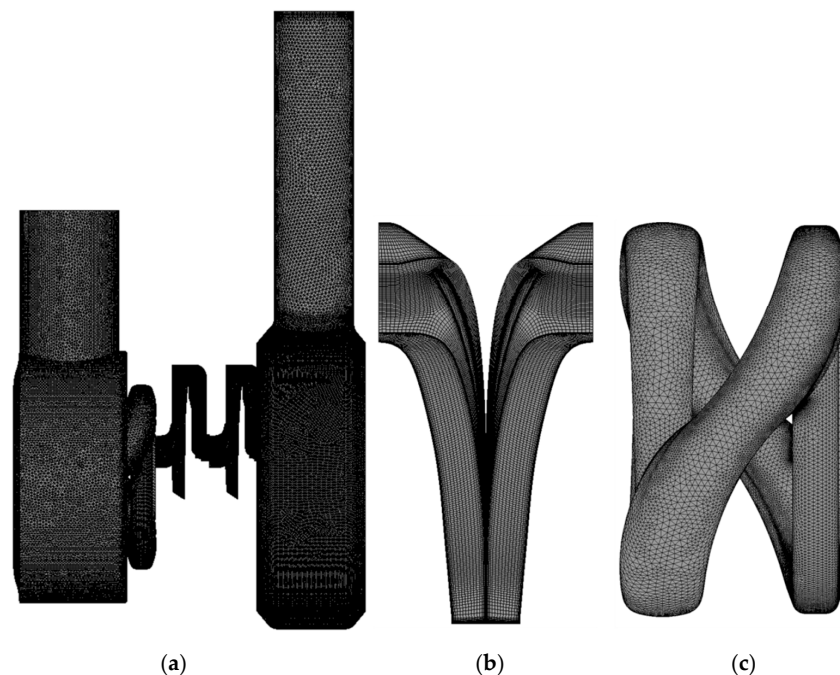


Figure 5. Meshes of (a) the entire model, (b) the double-suction impeller and (c) the twin volute.

4. Pump Performance

The theoretical performance of the pump design was shown in the previous section. The pump performance obtained from the CFD simulations is presented here. The head coefficient and efficiency curves were compared with the theoretical calculation for the initial validation of the CFD results. Figure 6 shows the pump characteristic curve comparison for the analytical and CFD studies. The efficiency curve was in good agreement with the analytical estimation. The higher efficiency obtained by the CFD simulations was due to the unaccounted losses in the simulations, such as the hydraulic and mechanical losses and the losses within the input and output sections of the pipe. The head obtained from the CFD results was within the range between the maximum and minimum head, as calculated theoretically for all flow rates. Thus, the efficiency and head curves obtained from the CFD simulations had an error percentage of less than 8%. Since this is a preliminary design feasibility study before manufacturing the pump for experimental analysis, the obtained CFD results are acceptable for further analysis.

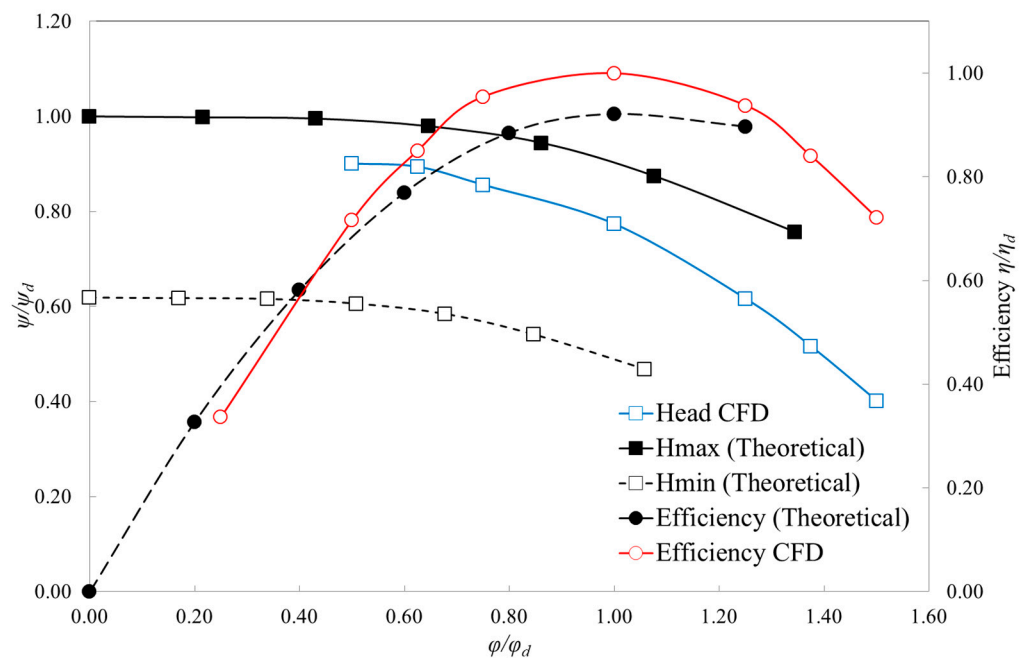


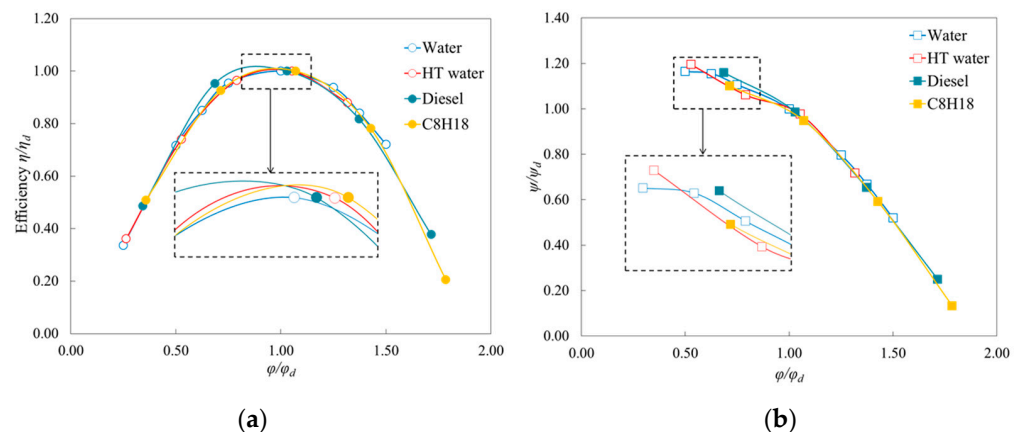
Figure 6. Performance comparison for theoretical and computational fluid dynamics (CFD) calculations.

The pump feasibility was tested for its operability with different chemicals used in chemical processing industries. Since normal water was used in the initial study, the pump was tested for water at a high temperature (116 °C) and pressure (1.73 bar). The viscosity of the water was reduced to 0.25 cP to imitate the conditions of a high-pressure boiler water pump. The centrifugal pump was also tested for hydrocarbons such as diesel ($C_{10}H_{22}l$) and debutanized diesel ($C_8H_{18}l$), which are common fluids pumped in petrochemical refineries. The material properties of the fluids were extracted at the fluid temperature obtained from the real site data where the pump would be installed. The dynamic viscosity, density and other fluid properties at the aforementioned particular temperature were applied to the CFD model. The simulations were carried out at an isothermal temperature and, hence, the conservation of energy equation was not solved [28,29]. The most relevant fluid properties are given in Table 2.

Table 2. Fluid properties.

Fluid Properties	Water	High-Temperature Water	Diesel (C ₁₀ H ₂₂ l)	C ₈ H ₁₈ l
Molar Mass [Kg/kmol]	18.02	18.02	142.285	114.231
Density [kg/m ³]	997	946.41	726.53	698.27
Temperature [°C]	25	116	240	177
Dynamic viscosity [cP]	1	0.25	0.22	0.125

The pump operating conditions were kept similar to the previous study for comparability. The head coefficient curves and efficiency curves for the different fluids are plotted in Figure 7. The flow coefficient was normalized by the design point of the reference fluid (water) such that $\varphi/\varphi_d = 1$ indicated the BEP of water. The efficiency curves of the low-viscous fluids had the same trend as that of the reference fluid. This means that the chemical pump could be operated in the same operating range with different fluids. However, the BEP of the low-viscous fluids shifted away from the BEP of water. The BEPs of the high-temperature water, diesel and C₈H₁₈ were shifted by +1%, −3.2% and +3.43%, respectively, compared with their water equivalent. The change in the BEP was associated with the change in density and viscosity of the fluid. It should be noted that the efficiency change for the different fluids was less than 1% at the BEPs of different fluids. Therefore, the pump performance did not degrade with the fluid change, but the operating point was shifted marginally. In other words, the system must be operated at lower flow rates in case of low-viscous fluids, in comparison with water, to ensure optimum performance.

**Figure 7.** (a) Pump efficiency and (b) head coefficient curves for multiple fluids.

The head curve also exhibited a similar trend for the fluids and fell within the theoretical head range. Compared to the reference fluid, the maximum deviation in the head curve was 2.7%, 0.45% and 5.4% for the high-temperature water, diesel and C₈H₁₈, respectively, at the low flow rate, which was an acceptable consequence. At the BEP, the head decreased by 17 m, 10 m and 38 m compared with the head at the BEP of water. This can be argued to be the result of the simultaneous effects of the viscosity on the efficiency and head of the pump. The overall operating point was slightly shifted toward the low flow rate for low-viscous fluids.

The circumferential area-averaged axial velocity along the pump impellers is plotted at the mid-span in Figure 8. The difference between the meridional velocity component and the radial velocity component implies a change in the axial velocity component. The magnitude of the axial velocity decreased from the leading edge to the trailing edge as the pressure gradient increased. The order of magnitude of the axial velocity was almost the same, relative to the mean radial velocity of 4.5 m/s at the mid-span of the impeller. A sudden spike in the axial velocity at the second stage impeller was observed at two

locations, indicating large recirculation in the area. This is discussed in the next section. The axial velocity component had the same magnitude for the low-viscosity fluids compared to water. This means that the pump was capable of handling low-viscous fluids without any large influence by the viscosity on the flow velocities. Therefore, it can be said that the proposed multistage pump design is feasible for the specific application which it is designed for in petrochemical processing plants.

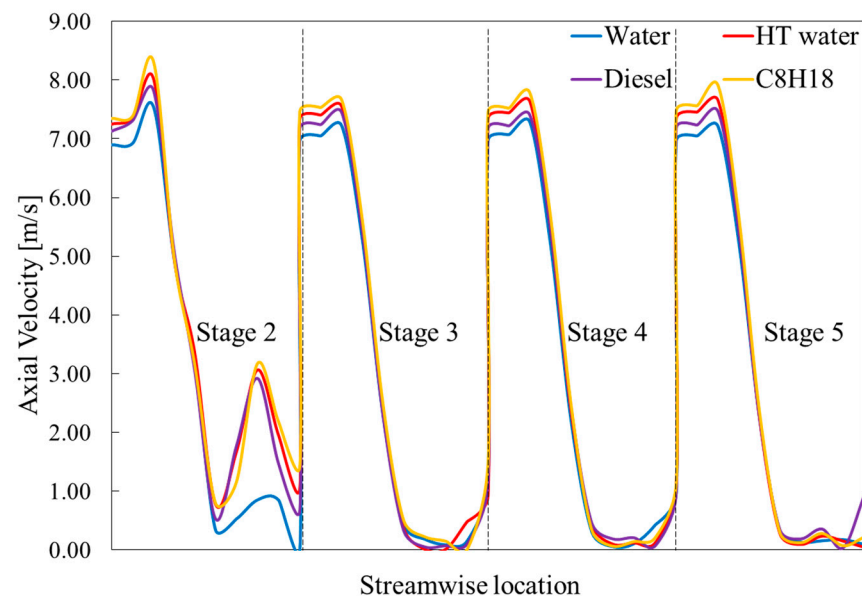


Figure 8. Axial velocity comparison along the impeller mid-span for Stages 2–5.

The design feasibility study using the CFD model only provided the initial hydraulic performance of the pump prior to the experimental studies. A laboratory-scale experimental analysis is required to investigate the actual performance of the pump using water and other chemicals.

5. Evaluation of Hydraulic Losses

The proposed multistage centrifugal pump was tested for its operability with multiple fluids of lower viscosities, and it was proven to be feasible. However, the design feasibility test of the pump could not be concluded without the loss analysis at each stage. To determine the head loss and efficiency loss, the normalized efficiency and head coefficient curves are plotted against the flow coefficient at each stage of the pump for water in Figure 9.

A significant decline was observed in the second stage for both the efficiency and head at higher flow rates. The efficiency obtained at $0.5 \varphi/\varphi_d$ was almost similar at all stages. As the flow rate increased, the efficiency followed a similar trend for Stages 1, 3, 4 and 5, while the efficiency at Stage 2 dropped significantly. The head also decreased at Stage 2, indicating huge pressure loss at this stage. The reason for the losses at the second stage needed to be investigated in-depth and design modifications must be advocated before manufacturing the pump.

The pump operating at the design point with water as the fluid was selected for the in-depth loss analysis. A trend graph is plotted at the impeller mid-span at each stage along the streamwise direction to identify the amount of losses in head and efficiency in Figure 10. The head and efficiency were divided by their maximum values for normalization. Stage 1 had two spikes due to the dual suction impeller design. It can be seen that the head dropped at the beginning of the second stage by 67% before rising again at the end of the stage. There was no drop in head observed in the rest of the stages. The maximum head was obtained at the end of the fifth stage impeller, which also corresponded to the

cumulative head of the entire pump. A similar drop in the efficiency curve was witnessed at the second stage. The dive in the efficiency curve at the beginning of each stage was due to the sudden change in the pressure gradient as the fluid moved from one stage to another. Although the efficiency dove at the leading edge of each impeller, it climbed back up immediately and rose sharply at the trailing edge. This was not the case with the second stage, where the efficiency remained the lowest throughout the blade streamwise. The elimination of losses at the second stage can improve the overall performance of the pump.

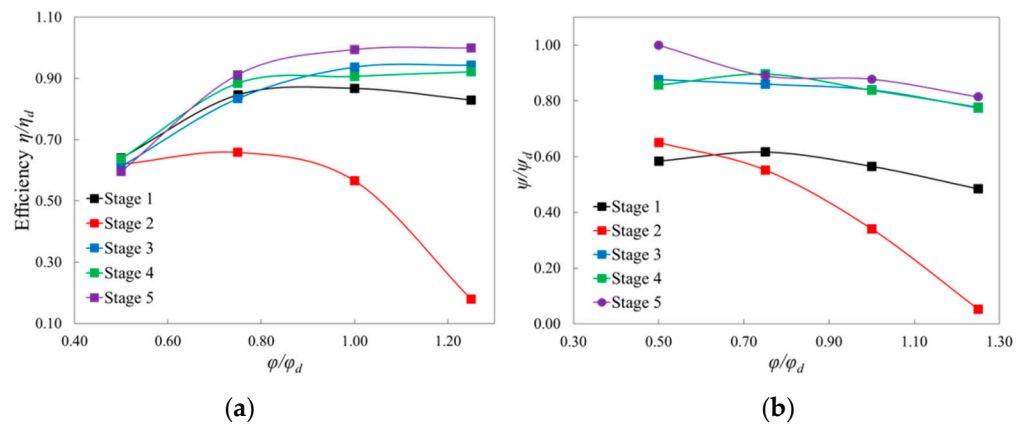


Figure 9. (a) Efficiency and (b) head coefficient curve of the individual stages for water.

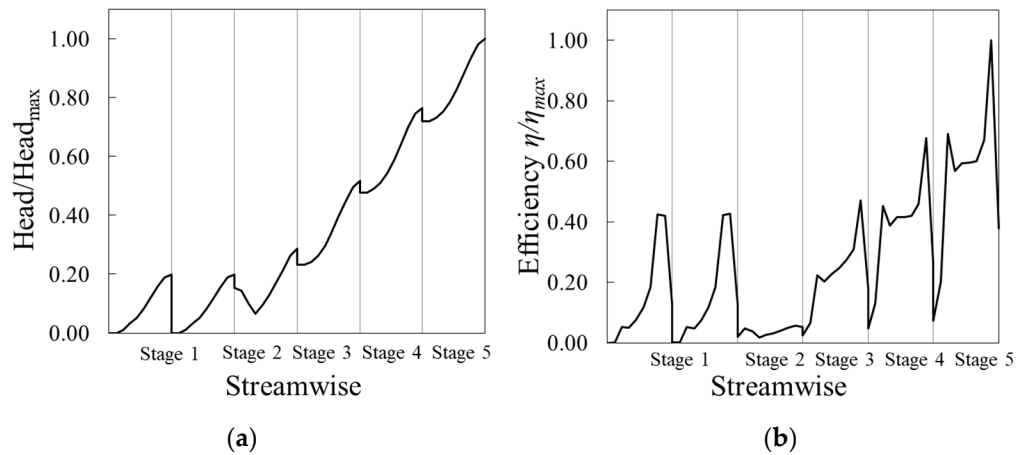


Figure 10. (a) Head and (b) efficiency trend graphs, plotted at the mid-span of the impellers for water at Q_d .

The blade loading curves for the impellers at Stages 2, 3, 4 and 5 are plotted in Figure 11. The normalized pressure was plotted along the streamwise direction at the design point for water. A pressure drop was observed at the leading edge of the second stage impeller, which recovered toward the trailing edge. The huge dive in the absolute pressure at the leading edge may succumb to cavitation in the long run. It is necessary to identify the source of the loss at the second stage. A drop in pressure at the pressure side of the impeller was observed at the 20% streamwise location, as marked in Figure 11. A severe pressure drop at this location indicates an obstruction to the flow at the pressure side. The pressure and velocity contours at the meridional plane of the blade are shown in Figure 12. A low-pressure region could be found at approximately the 20% streamwise location, and the corresponding low-velocity region confirmed the formation of a stagnation zone, causing blockage to the flow.

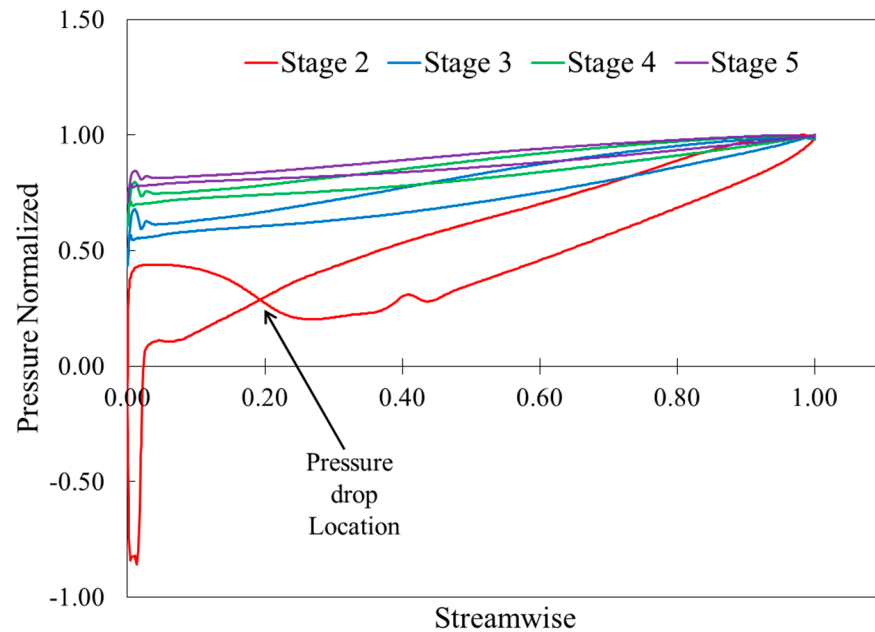


Figure 11. Blade loading at the mid-span of the impeller at each stage for water at the design point.

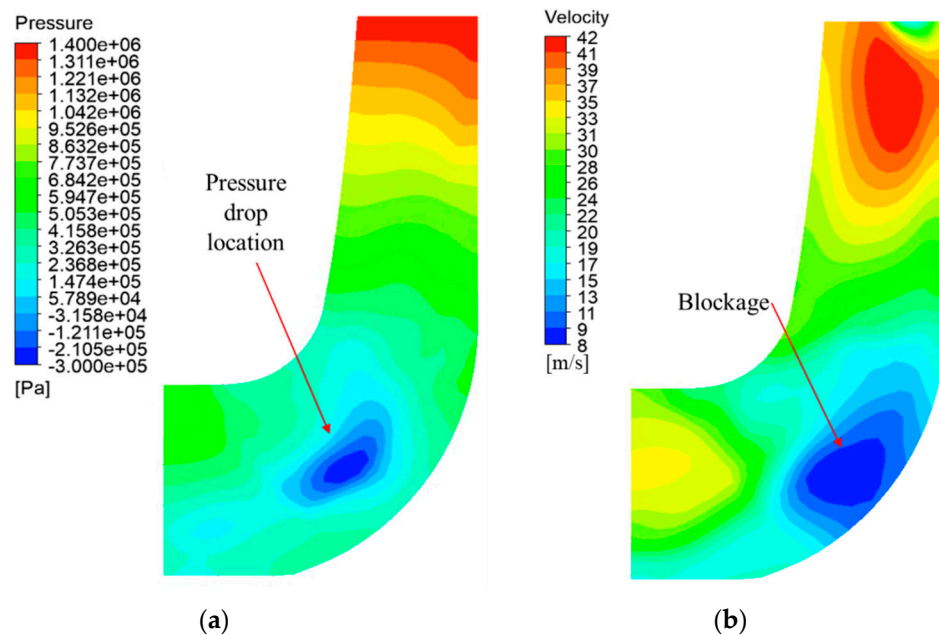


Figure 12. Contours at the meridional plane of the second stage impeller for (a) pressure and (b) velocity in a stationary frame.

The velocity streamlines at the mid-span from a blade-to-blade view of the impellers at each stage is shown in Figure 13. The fluid flowed along the blade angle for all stages except for Stage 2. The fluid incidence angle was found to be larger than 90° to the second stage impeller blade angle. The fluid exhibited chaotic behavior in the impeller region, which accounts for the losses discovered earlier. The turbulent behavior of the fluid at the second stage impeller was, however, not carried over to the next stage. The diffuser and return vane at the second stage corrected the flow instabilities and prepared the fluid incidence angle tangent to the next stage blade angle.

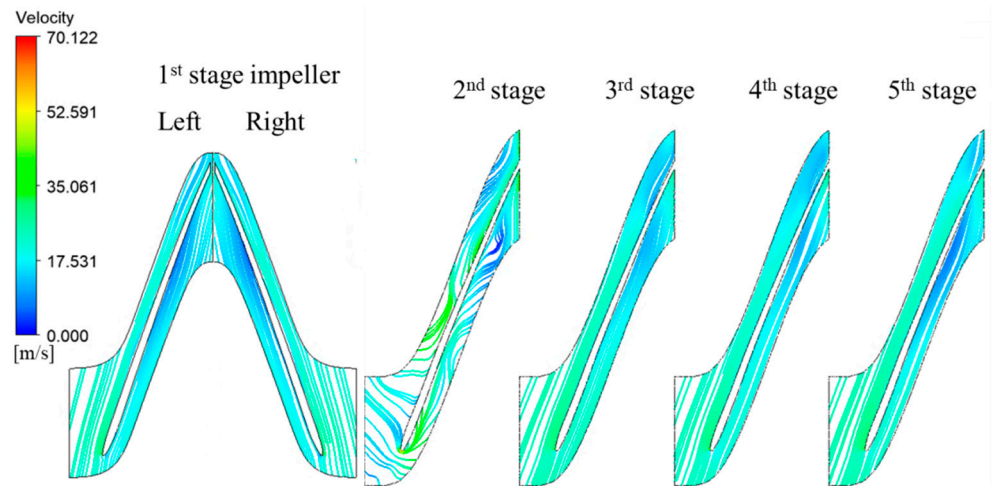


Figure 13. Blade-to-blade views of the velocity streamlines at the midspan of the impellers at each stage. The left and right impellers at the first stage indicate the double-suction impeller.

The disparity between the fluid incidence angle and the blade angle at the second stage impeller was due to the incoming flow from the volute. The fluid entering the volute from the first stage impeller split into the two arms of the 180° staggered twin volute, flowed along the volute surfaces and rejoined toward the volute exit. The fluid at the volute exit was observed to have a larger radial force than the axial force and, as a result, created a pre-swirl at the inlet of the second stage impeller. This pre-swirl of the fluid was responsible for the imbalance in the flow angles and the losses associated with it.

The velocity triangle diagram of the flow at the inlet of the impellers is shown in Figure 14. Theoretically, at the design flow rate, the fluid reached the impeller radially without any swirl. The absolute fluid velocity at the inlet creates an angle of $\alpha = 90^\circ$ with the direction of the blade rotation in an ideal case. However, these assumptions are not likely to conform to an actual centrifugal pump [30]. The absolute flow angle decreased sharply to 12.68° , and the relative flow angle increased to form an obtuse angle of 121.6° at the second stage impeller. This was due to the high absolute velocity at the impeller inlet caused by the large circumferential velocity component of the flow exiting the volute.

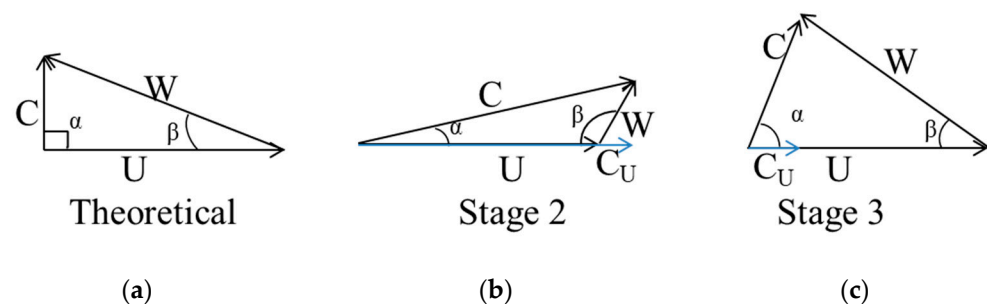


Figure 14. (a) Theoretical, (b) Stage 2 and (c) Stage 3 velocity triangles at the impeller inlet.

Figure 15 shows the 3D velocity streamlines at the volute–impeller interface, indicating a significant shift in the flow direction. As mentioned above, it can be seen that the circumferential velocity increased excessively due to the outlet shape of the first stage volute. The absolute flow angle at the inlet of the Stage 3 impeller was 25% lower than the ideal case due to the swirl velocity observed at the inlet, which was formed by the return vanes of the second stage. Here, the second stage return vanes acted as an inlet guide vane to the third stage impeller. The velocity triangle diagrams of Stage 4 and 5 impellers are similar to the Stage 3 impeller.

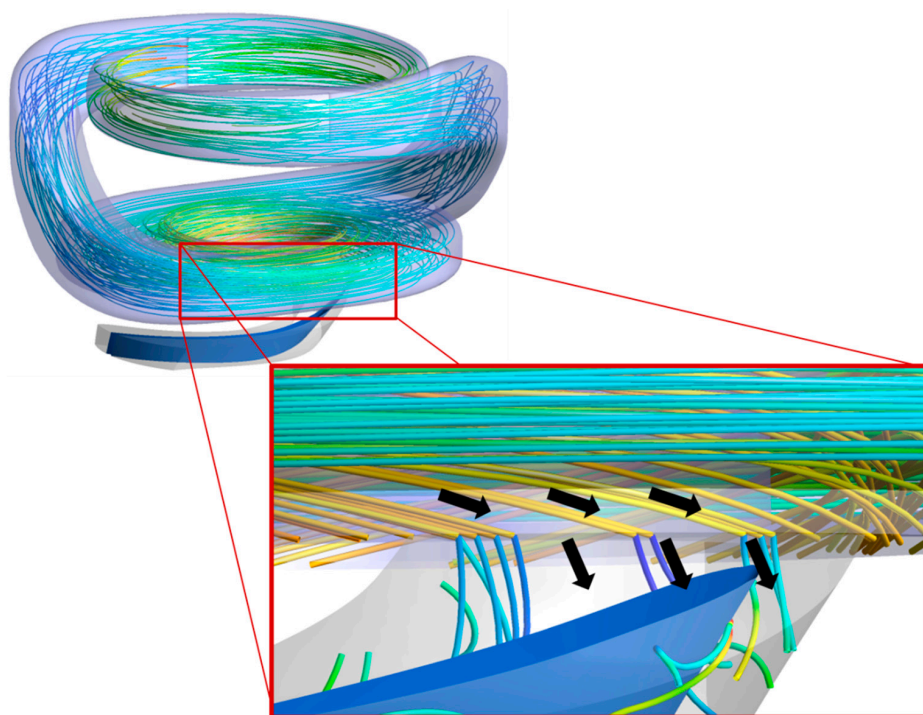


Figure 15. 3D velocity streamlines at the volute–impeller interface (Stage 1–Stage 2 interface).

The cause of the losses at the second stage was identified as the sudden change in the flow angle at the volute–impeller interface due to a high radial force from the volute. The effect of this was visualized by identifying the vortex core region formed inside the impeller. The velocity streamlines and the vortex core with a swirling strength of 0.004 are shown in Figure 16. The majority of the vortices were formed at the pressure side of the impeller, causing blockage to the incoming flow. They were formed due to the flow separation at the leading edge. These vortices could be suppressed by regulating the incoming flow from the volute.

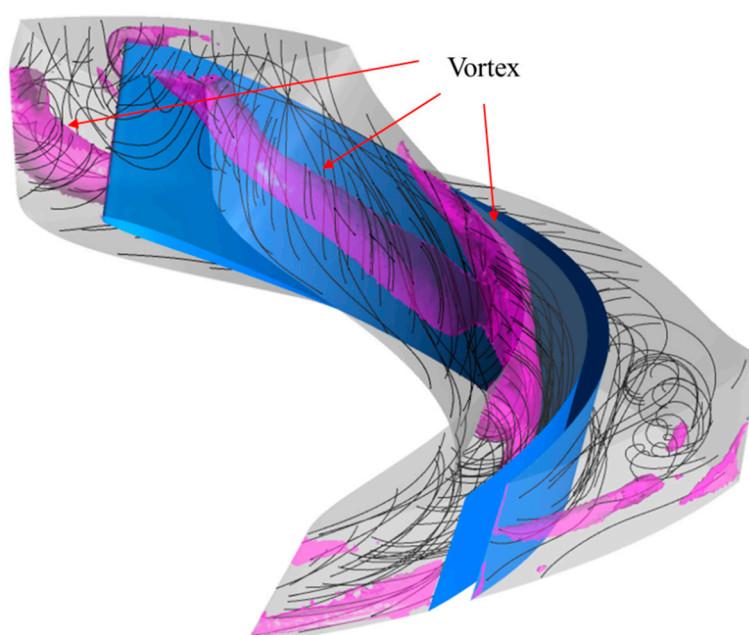


Figure 16. Velocity streamlines and vortex core region (swirling strength = 0.004).

To address the losses at the second stage, we provide certain design recommendations to pump manufacturers:

1. The pre-swirl observed at the volute exit must be suppressed by reducing the large radial forces of the fluid flowing through the twin volute. This may be possible with the installation of a baffle plate at the exit of the twin volute, similar to the baffle plates installed in the suction chamber before the inlet of the first-stage impeller. In engineering practice, to eliminate the pre-swirl component, baffles are typically inserted in the channels between the stages of multistage pumps, thus reducing incidence losses for the next stage impeller [31]. Baffles can de-swirl the incoming flow at the second-stage inlet. A similar anti-swirl device was used by Schoot et al. [32] to decrease the pre-swirl from a twin-volute crossover section;
2. The disparity between the flow angle and the impeller incidence angle must be corrected to obtain a uniform flow through the impeller. An additional stationary guide vane installation is recommended between the first-stage volute and the second-stage impeller, whose exit angle is tangent to the impeller blade angle. Several guide vane designs were tested at the inlet of single-stage centrifugal pumps and were found to be effective in regulating the pre-swirl [33–35]. Similar guide vane designs can be incorporated ahead of the second-stage impeller. Numerical optimization is required to find the optimum guide vane design that regulates the pre-swirl without performance degradation of the pump.

6. Conclusions

A five-stage centrifugal pump with a double-suction impeller and a twin volute was designed for application in chemical industries. A CFD model of the pump was created for the design feasibility test of the pump. The pump characteristics were studied theoretically and compared with CFD simulations for initial validation of the CFD model. The operability of the pump to handle hazardous and low-viscous fluids was tested using this model. A loss analysis at the design point was conducted to find the losses associated with the proposed pump design. The head and efficiency losses at the second stage were found to be higher than in the other stages. The incidence angle of the incoming flow at the second-stage impeller was not tangential to the blade angle, which was responsible for the losses at the second stage. The incoming flow from the twin volute had large radial forces, which caused a pre-swirl at the interface between the first and second stage. This pre-swirl caused divergence in the flow angle at the impeller inlet. Vortices were formed as a result of the flow separation at the leading edge. This led to a pressure drop at the pressure side of the impeller, giving rise to flow blockages. The in-depth flow physics of fluid behavior is explained in this paper. Design recommendations to diminish the losses and improve the overall performance of the pump are provided. The implementation of these recommendations will be the subject of future works of this study. The improved pump design would be tested using the experimental set-up on a laboratory scale. The design parameters of the impeller, diffuser, return vane and the twin volute can be subjected to optimization studies for a performance upgrade. This study benefits pump manufacturers and designers for effectively designing multistage centrifugal pumps intended for pumping low-viscous, volatile and flammable fluids with high head and flow rate requirements in the chemical processing industry.

Author Contributions: Conceptualization, J.-H.K., S.-B.M. and M.M.S.; methodology, S.-B.M. and M.M.S.; software, M.M.S.; validation, J.-H.Y. and M.M.S.; formal analysis, S.-B.M. and M.M.S.; investigation, S.K., S.-B.M. and M.M.S.; resources, J.-H.Y., K.-H.L. and C.J.; data curation, M.M.S. and S.-B.M.; writing—original draft preparation, M.M.S.; writing—review and editing, S.-B.M. and M.M.S.; visualization, M.M.S.; supervision, J.-H.K.; project administration, K.-H.L.; funding acquisition, J.-H.K. and K.-H.L. All authors have read and agreed to the published version of the manuscript.

Funding: This research was supported by grants (No. EE200001) and (No. JB210001) of the Korea Institute of Industrial Technology (KITECH).

Institutional Review Board Statement: Not applicable.

Informed Consent Statement: Not applicable.

Conflicts of Interest: The authors declare no conflict of interest.

References

1. American Petroleum Institute. *API 610-Centrifugal Pumps for Petroleum, Heavy Duty Chemical, and Gas. Industry Services*, 8th ed.; American Petroleum Institute: Washington, DC, USA, 2003.
2. Bellary, S.A.I.; Samad, A. Pumping crude oil by centrifugal impeller having different blade angles and surface roughness. *J. Pet. Explor. Prod. Technol.* **2016**, *6*, 117–127. [[CrossRef](#)]
3. Bellary, S.A.I.; Samad, A. Improvement of Efficiency by Design Optimization of a Centrifugal Pump Impeller. In Proceedings of the ASME Turbo Expo 2014, Turbine Technical Conference and Exposition Turbomachinery, Düsseldorf, Germany, 16–20 June 2014; Volume 2D. [[CrossRef](#)]
4. Bellary, S.A.I.; Adhav, R.; Siddique, M.H.; Chon, B.H.; Kenyery, F.; Samad, A. Application of computational fluid dynamics and surrogate-coupled evolutionary computing to enhance centrifugal-pump performance. *Eng. Appl. Comput. Fluid Mech.* **2016**, *10*, 171–181. [[CrossRef](#)]
5. Siddique, M.H.; Bellary, S.A.I.; Samad, A.; Kim, J.H.; Choi, Y.S. Experimental and Numerical Investigation of the Performance of a Centrifugal Pump When Pumping Water and Light Crude Oil. *Arab. J. Sci. Eng.* **2017**, *42*, 4605–4615. [[CrossRef](#)]
6. Siddique, M.H.; Afzal, A.; Samad, A. Design Optimization of the Centrifugal Pumps via Low Fidelity Models. *Math Probl. Eng.* **2018**. [[CrossRef](#)]
7. Siddique, M.H.; Mrinal, K.R.; Samad, A. Optimization of a Centrifugal Pump Impeller by Controlling Blade Profile Parameters. In Proceedings of the ASME Turbo Expo 2016: Turbomachinery Technical Conference and Exposition, Turbomachinery, Seoul, Korea, 13–17 June 2016; Volume 2C. [[CrossRef](#)]
8. Watanabe, H.; Yamashita, T.; Watanabe, S.; Hara, Y. CFD Analysis of Axial Thrust in Three Stages Centrifugal Pump at Design and Part load Conditions. In Proceedings of the ASME/JSME/KSME 2015 Joint Fluids Engineering Conference, Symposia, Seoul, Korea, 26–31 July 2015; Volume 1A, Part 2. [[CrossRef](#)]
9. Takamine, T.; Furukawa, D.; Watanabe, S.; Watanabe, H.; Miyagawa, K. Experimental Analysis of Diffuser Rotating Stalling a Three-Stage Centrifugal Pump. *Int J. Fluid Mach. Syst.* **2018**, *11*, 77–84. [[CrossRef](#)]
10. Coker, A.K. *Ludwig's Applied Process Design for Chemical and Petrochemical Plants*, 4th ed.; Gulf professional publishing: Houston, TX, USA, 2014; Volume 1, pp. 303–370.
11. McGuire, J.T. Centrifugal pumps. In *Pumps for Chemical Processing*; CRC Press: Boca Raton, FL, USA, 2019; pp. 27–105.
12. Song, Y.; Fan, H.; Zhang, W.; Xie, Z. Flow Characteristics in Volute of a Double-Suction Centrifugal Pump with Different Impeller Arrangements. *Energies* **2019**, *12*, 669. [[CrossRef](#)]
13. González, J.; Fernández Oro, J.M.; Díaz, K.M.A.; Blanco, E. Unsteady Flow Patterns for a Double Suction Centrifugal Pump. *ASME J. Fluids Eng.* **2009**, *131*, 071102. [[CrossRef](#)]
14. Zhang, Z.C.; Wang, F.J.; Yao, Z.F.; Leng, H.F.; Zhou, P.J. Investigation on Impeller Radial Force for Double-Suction Centrifugal Pump with Staggered Blade Arrangement. In Proceedings of the 6th International Conference on Pumps and Fans with Compressors and Wind Turbines, Beijing, China, 19–22 September 2013. [[CrossRef](#)]
15. Li, Q.; Wu, D. Study on the Reduction of Pressure Fluctuation for a Double-Suction Centrifugal Pump with Staggered Blades. In Proceedings of the ASME 2018 5th Joint US-European Fluids Engineering Division Summer Meeting, Montreal, QC, Canada, 15–20 July 2018. [[CrossRef](#)]
16. Kang, C.; Li, Y. The effect of twin volutes on the flow and radial hydraulic force production in a submersible centrifugal pump. *Proc. Inst. Mech. Eng. Part A* **2015**, *229*, 221–237. [[CrossRef](#)]
17. Mina, E.M.; Abdelmessih, R.N.; Matbouly, M.E. Reduction of Radial Thrust by Using Triple-Volute Casing. *Ain Shams Eng. J.* **2019**, *10*, 721–729. [[CrossRef](#)]
18. Suzuki, T.; Takemura, T. CFD Analysis of Performance of Five-Stage High-Pressure Volute Pump. In Proceedings of the 17th Symposium on Turbomachinery Flow Simulation and Optimization, Washington, DC, USA, 10–14 July 2016; Volume 1A. [[CrossRef](#)]
19. Teesink, P.; Visser, F.; Jochems, J. Efficiency Optimization of a 30MW Main Boiler Feedwater Pump Using CFD and Scaled Model Tests. In Proceedings of the 25th Symposium on Fluid Machinery, Incline Village, NV, USA, 7–11 July 2013; Volume 1B. [[CrossRef](#)]
20. Zhang, X.; Huang, H. Flow field analysis of multi-stage middle-open centrifugal pump inter-stage flow passage. In Proceedings of the 2nd International Symposium on Hydrogen Energy and Energy Technologies (HEET 2019), Osaka, Japan, 12–13 December 2019. [[CrossRef](#)]
21. ANSYS. *ANSYS TurboSystem User's Guide, ANSYS BladeModeler; Software Handbook*; ANSYS: Fort Cannon, PA, USA, 2013.
22. Zhu, J.; Banjar, H.; Xia, Z.; Zhang, H.Q. CFD simulation and experimental study of oil viscosity effect on multi-stage electrical submersible pump (ESP) performance. *J. Pet. Sci. Eng.* **2016**, *146*, 735–745. [[CrossRef](#)]

23. Nourbakhsh, A.; Jaumotte, A.; Hirsch, C.; Parizi, H.B. Affinity laws. In *Turbopumps and Pumping Systems*; Springer: Berlin/Heidelberg, Germany, 2008; p. 35. [[CrossRef](#)]
24. Menter, F. Innovative Turbulence Modeling: SST Model in ANSYS CFX. Available online: <http://www.ansys.com/assets/tech-briefs/cfx-sst.pdf> (accessed on 15 December 2020).
25. Kim, J.H.; Cho, B.M.; Kim, S.; Lee, Y.K.; Choi, Y.S. Detailed flow characteristic analysis of a three-stage centrifugal pump at design and off-design conditions. In *IOP Conference Series: Earth and Environmental Science*; IOP Publishing: Bristol, UK, 2019; Volume 240, p. 092004. [[CrossRef](#)]
26. Kim, J.H.; Cho, B.M.; Kim, S.; Lee, Y.K.; Choi, Y.S. Steady and Unsteady Flow Characteristics of a Multi-stage Centrifugal Pump under Design and Off-design Conditions. *Int. J. Fluid Mach. Syst.* **2019**, *12*, 64–70. [[CrossRef](#)]
27. Maleki, A.; Ghorani, M.M.; Haghghi, M.H.S.; Riasi, A. Numerical study on the effect of viscosity on a multistage pump running in reverse mode. *Renew. Energy* **2020**, *150*, 234–254. [[CrossRef](#)]
28. Shi, Y.; Zhu, H.; Zhang, J.; Zhang, J.; Zhao, J. Experiment and numerical study of a new generation three-stage multiphase pump. *J. Pet. Sci. Eng.* **2018**, *169*, 471–484. [[CrossRef](#)]
29. Ofuchi, E.M.; Stel, H.; Sirino, T.; Vieira, T.S.; Ponce, F.J.; Chiva, S.; Morales, R.E.M. Numerical investigation of the effect of viscosity in a multistage electric submersible pump. *Eng. Appl. Comput. Fluid Mech.* **2017**, *11*, 258–272. [[CrossRef](#)]
30. Fox, R.W.; Pritchard, P.J.; McDonald, A.T. *Fox and McDonald's Introduction to Fluid Mechanics*; John Wiley & Sons, Inc.: Hoboken, NJ, USA, 2020.
31. Osman, K.M.; Wang, W.; Yuan, J.; Zhao, J.; Wang, Y.; Liu, J. Flow loss analysis of a two-stage axially split centrifugal pump with double inlet under different channel designs. *Proc. Inst. Mech. Eng. Part C* **2019**, *233*, 5316–5328. [[CrossRef](#)]
32. Schoot, M.V.D.; Visser, F. Efficiency Upgrade of a Double-Case Pump Using CFD-Based Design Optimization and Scaled Model Tests. In Proceedings of the ASME/JSME/KSME 2015 Joint Fluids Engineering Conference, Symposia, Seoul, Korea, 26–31 July 2015; Volume 1. [[CrossRef](#)]
33. Lin, P.; Li, Y.; Xu, W.; Chen, H.; Zhu, Z. Numerical Study on the Influence of Inlet Guide Vanes on the Internal Flow Characteristics of Centrifugal Pump. *Processes* **2020**, *8*, 122. [[CrossRef](#)]
34. Tan, L.; Cao, S.; Wang, Y.; Zhu, B. Influence of axial distance on pre-whirl regulation by the inlet guide vanes for a centrifugal pump. *Sci. China Technol. Sci.* **2012**, *55*, 1037–1043. [[CrossRef](#)]
35. Liu, M.; Tan, L.; Cao, S. Influence of Geometry of Inlet Guide Vanes on Pressure Fluctuations of a Centrifugal Pump. *J. Fluid Eng.* **2018**, *140*, 091204. [[CrossRef](#)]